American Mineralogist, Volume 76, pages 343–353, 1991

The identification of naturally occurring TiO_2 (B) by structure determination using high-resolution electron microscopy, image simulation, and distance-least-squares refinement

JILLIAN F. BANFIELD,* DAVID R. VEBLEN
Department of Earth and Planetary Sciences, The Johns Hopkins University, Baltimore, Maryland 21218, U.S.A.
DAVID J. SMITH
Center for Solid State Science and Department of Physics, Arizona State University, Tempe, Arizona 85287, U.S.A.

ABSTRACT

Semicoherently intergrown lamellae of a new TiO_2 mineral have been identified in anatase crystals from Binntal, Valais, Switzerland. This unnamed mineral has been reported previously as the synthetic polymorph TiO_2 (B) (Marchand et al., 1980). We have interpreted high-resolution electron micrographs to determine the positions of columns of Ti cations within the unit cell as determined by electron diffraction. The model structure, which consisted of Ti cations octahedrally coordinated by O, was tested by comparing computer-generated images with experimental micrographs from two orientations. Simulations were calculated for defocus and thickness conditions necessary to match the experimental and calculated images of the host anatase. The model structure was then refined using a distance-least-squares (DLS) program to adjust all interatomic distances simultaneously to values comparable with those found in anatase and rutile. The image simulations for this DLS-improved structure match the experimental images for both orientations. The DLS-improved model closely reproduces the detailed polyhedral distortions from the ideal structure that were predicted by Catlow et al. (1984) using energy minimization techniques. The TiO_2 (B) structure, composed of edge- and corner-linked pairs of edge-sharing octahedra, can be generated from the anatase structure by regular shear parallel to (103) of anatase, which is the observed orientation of the interface between the two minerals. High-resolution heating experiments carried out within the electron microscope showed that the TiO_2 (B) polymorph was converted to anatase either by growth of steps (<1 nm high) on the lamellar margins that removed the shear component relating the two structures, or by a bulk mechanism when anatase nuclei were scarce or absent. This reaction occurs in the microscope at a furnace temperature of approximately 700 °C, approximately 100 °C below the anatase-rutile transformation. The irreversible TiO_2 (B) → anatase and anatase → rutile reactions may be useful indicators of peak temperatures if it can be established that both minerals are common in low-grade metamorphic rocks.

INTRODUCTION

There are seven known polymorphs of TiO_2, six of which have distinct structures (Table 1). Three of these polymorphs, rutile, anatase, and brookite have been found previously in nature. In this paper we report the characterization of lamellae of a polymorph, currently known as TiO_2 (B) (Marchand et al., 1980), which has been found in natural anatase crystals.

Because these lamellae occupy a small volume of the anatase crystals, our attempt to characterize their structure using X-ray precession photographs was unsuccessful. Consequently, we applied a number of electron microscopic techniques to derive a structural model, adjusted the model until computer image simulations approximately matched the atomic-resolution images, and finally refined the model using a distance-least-squares (DLS) structure modeling program. This approach is thus shown to be a useful alternative to those of Catlow et al. (1984) and Theobald et al. (1984) for solving structures when only small quantities of material are available. Previous methods combine electron or powder X-ray diffraction with energy minimization modeling based on the Born model for the ionic solid. However, they do not take advantage of the capabilities of very high-resolution electron microscopes that produce images which are interpretable using image simulation techniques (O'Keefe, 1984) in terms of atomic positions.

The nature of grain boundaries between different phases is of considerable interest because the structure of these

* Present address: Department of Geology and Geophysics, University of Wisconsin–Madison, 1215 West Dayton Street, Madison, Wisconsin 53706, U.S.A.

0003–004X/91/0304–0343$02.00

TABLE 1. List of the TiO_2 polymorphs with distinct structures

Structure	Space group	Density ($g \cdot cm^{-3}$)	Unit cell data (nm)	Reference
Rutile	$P4_2/mnm$	4.13	$a = 0.459$, $c = 0.296$	Cromer and Herrington (1955)
Anatase	$I4_1/amd$	3.79	$a = 0.379$, $c = 0.951$	Cromer and Herrington (1955)
Brookite	$Pbca$	3.99	$a = 0.917$, $b = 0.546$, $c = 0.514$	Baur (1961)
TiO_2 (B)	$C2/m$	3.64	$a = 1.216$, $b = 0.374$, $c = 0.651$, $\beta = 107.29°$	Marchand et al. (1980)
TiO_2 II	$Pbcn$	4.33	$a = 0.452$, $b = 0.550$, $c = 0.494$	Simons and Dachille (1967)
TiO_2 (H)	$I4/m$	3.46	$a = 1.018$, $c = 0.297$	Latroche et al. (1989)

Note: The $CaCl_2$ structure is related to that of rutile by a second order phase transformation.

boundary regions controls diffusion rates and transformation mechanisms. Based on interpretation of atomic-resolution images, it is possible to deduce the bonding configuration at the boundary between the anatase and TiO_2 (B)–phase. Furthermore, the obvious structural relationship between these phases, first noted by Brohan et al. (1982), can be used to interpret images with near atomic-level resolution that show the phase transformation mechanism observed directly (at high temperature) in the electron microscope.

Sample description and experimental methods samples

The anatase crystals examined in this study are from two localities near Binntal, Valais, Switzerland (46°20′N, 8°12′E). The first sample was from the collection of Howard Belsky. The second sample was from the collection of Carl Bosch, U.S. National Museum, Division on Mineralogy, Smithsonian Institution, Washington, DC (Museum Number B6134) and is from the Alp Lercheltini area. The anatase crystals occur in a mica-rich gray paragneiss that experienced upper greenschist facies metamorphism approximately 30–40 Ma (S. Graeser, written communication). Graeser states that the anatase clearly formed after the climax of metamorphism and suggests a date based on K-Ar determinations for fissure minerals of approximately 11 m.y. Electron microprobe analyses for both samples (K. Livi, analyst) show them to be >99% TiO_2 with small amounts of Fe and Al, and traces of Mn and Cr. No compositional difference between the coexisting polymorphs could be detected using either analytical electron microscopy (AEM) or by repeated electron microprobe analyses from crystals known to contain lamellae. When examined optically (using reflected and transmitted light microscopy), the crystals appear to be homogeneous, coarsely twinned anatase.

X-ray diffraction

Single crystal X-ray diffraction patterns were obtained with a precession camera using Zr-filtered Mo$K\alpha$ X-rays. Zero- and first-level b-axis films were exposed for up to 1 week to enhance possible weak reflections associated with the TiO_2 (B)–phase. Although reflections attributable to the B-phase were not detected in these experiments, a careful powder X-ray diffraction study by J. Post revealed that small diagnostic TiO_2 (B) peaks could be identified in sample B6134.

Electron microscopy

The anatase and lamellae were initially characterized using a Philips 420T transmission electron microscope (TEM) operated at 120 keV. Samples were prepared by crushing small crystals; a suspension of the material in alcohol was deposited on a holey carbon grid. Selected-area electron diffraction (SAED) patterns and convergent-beam electron diffraction (CBED) patterns were obtained both from thin edges of crystals containing anatase and lamellae and from areas comprised only of lamellae. AEM data were obtained using an EDAX Li-drifted Si detector with a Be window and analyzed using a Princeton Gamma-Tech System IV X-ray system.

High-resolution electron micrographs were recorded with a 400-keV JEM 4000EX TEM with a point resolution of close to 0.17 nm (Cs = 1.0 mm). Through-focus series were recorded for two orientations at magnifications of 500 000 and 800 000×.

Heating experiments were carried out on crushed grains mounted on holey carbon films. The sample was heated to a furnace temperature of 800 °C in a single-tilt H_2O-cooled Gatan holder. In some cases, partly reacted oriented crystals were examined by transferring the sample to a double-tilt holder after cooling.

Computer-simulated images for anatase and model structures were calculated using the SHRLI programs version 80F (O'Keefe et al., 1978; O'Keefe, 1984; Self and O'Keefe, 1988).

Distance-least-squares refinement

The DLS refinement was carried out using the DLS-76 program originally written by C. H. Baerlocher and A. Hepp, revised by Brund Guigas, and adapted for an IBM computer by S. L. Lawton and E. L. Wu. The DLS procedure is described by Burnham (1985).

Results

Sample characterization

Both anatase samples contained lamellae of the same second mineral. The samples differed only slightly in the abundance of the second phase (the Smithsonian sample contained slightly more lamellae). Data presented below were obtained from, and are appropriate for, both samples.

The electron micrograph in Figure 1 shows a crystal of anatase in the [010] projection that contains lamellae of

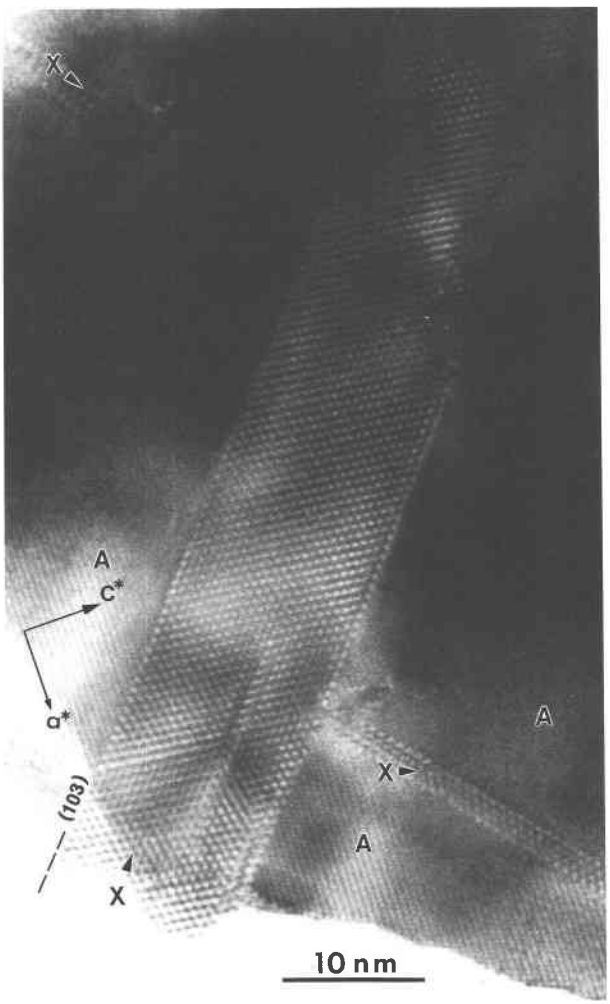

Fig. 1. Transmission electron micrograph down [010] of anatase (A) showing two sets of lamellae of a second mineral X parallel to {103} of anatase.

the second mineral labeled "X," which is shown below to be TiO_2 (B). The margins of the lamellae are parallel to the symmetrically equivalent {103} planes of anatase. In most areas, the lamellae were observed in only one of these two directions. Based on the absence of reflections in X-ray precession photographs, the weakness of peaks in powder X-ray diffraction traces, and the projected areas of lamellae in TEM images, it is estimated that the lamellae occupy less than 1% of the sample. They range from a few nanometers to hundreds of nanometers across. SAED and CBED patterns indicate that the lamellae have a three-dimensional reciprocal lattice distinct from those of anatase, rutile, and brookite. Furthermore, the image characteristics extend to the edge of the sample (Fig. 2), indicating that the distinct unit cell is not the result of twinning or a moiré effect.

SAED patterns such as those in Figure 3 show that the reciprocal lattices of the two minerals have a well-defined orientation relationship. Figure 2 indicates that the interface is parallel to (103) anatase. The presence of a reflection from the lamellae just inside the 103 reflection of anatase indicates that the interplanar spacings of lattice planes parallel to the interface are not exactly equal. Moreover, from Figure 3b it is apparent that the $\bar{1}1\bar{2}$ reflection of anatase associated with the pseudo-close-packed planes almost exactly overlies a reflection from the lamellar phase. The SAED patterns indicate that there is misfit between the lamellae and anatase along their interface so that the intergrowth is probably semicoherent. The *d*-values measured from the electron diffraction patterns are listed in Table 2.

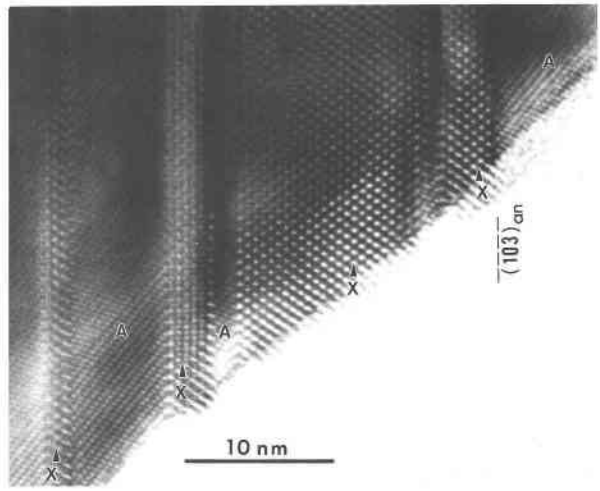

Fig. 2. Image down [010] of the intergrown minerals showing areas of anatase (A) and a second mineral (X).

TABLE 2. List of *d*-values measured from SAED patterns, calculations for TiO_2 (B), and indices

d_{meas} this study	*d*-TiO_2 (B) calculated*	*hkl*
6.2	6.22	001
5.8	5.80	200
5.1	5.06	$20\bar{1}$
3.7	3.73	201
3.3	3.22	$11\bar{1}$
3.2	3.16	$20\bar{2}$
3.2	3.14	$\bar{2}10$, 210
3.1	3.11	002
3.0	2.99	$40\bar{1}$
3.0	2.97	111, $11\bar{1}$
2.9	2.90	400
2.7	2.69	310, $\bar{3}10$
2.6	2.68	311, $31\bar{1}$
2.6	2.53	$40\bar{2}$
2.5	2.45	202
2.5	2.45	$11\bar{2}$
2.4	2.37	401
2.3	2.30	$3\bar{1}1$, 311
2.2	2.28	$\bar{3}12$, $31\bar{2}$
2.2	2.17	$20\bar{3}$
2.1	2.07	003
2.0	2.03	$51\bar{1}$
2.0	2.03	$\bar{5}11$
2.0	2.03	$60\bar{1}$

* Calculated from the cell dimensions given by Marchand et al. (1980).

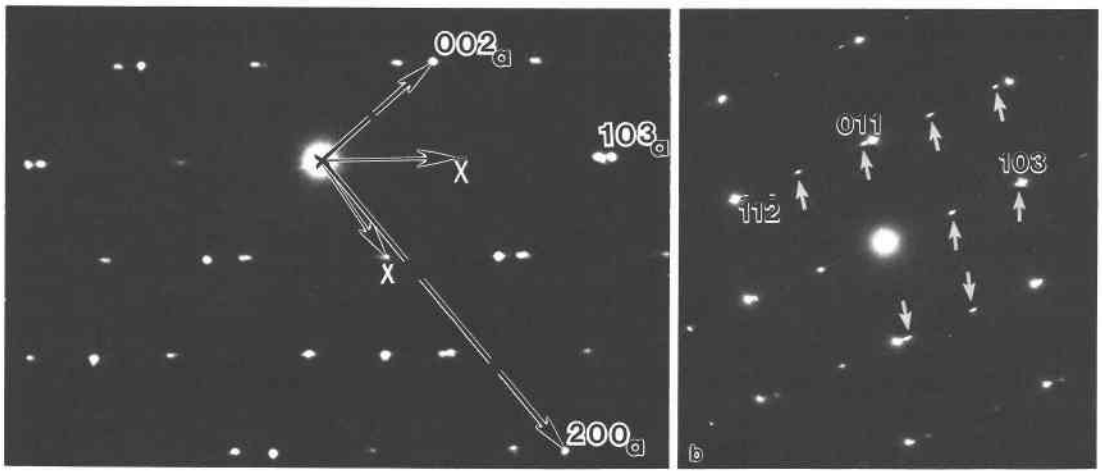

Fig. 3. SAED patterns (**a**) showing [010] of anatase and the reciprocal lattice from mineral X in lamellae coexisting with anatase; (**b**) in [31$\bar{1}$] of anatase, showing the relative orientation of the two reciprocal lattices. Reflections from mineral X are arrowed.

In situ heating experiments

A series of heating experiments was carried out within the Philips 420T electron microscope. Since these studies involved the use of crushed grains on holey carbon films, the exact temperature achieved was not known. In general, a reaction was observed at a furnace temperature of approximately 700 °C for crystals that were located close to the bars of the Cu support grid. In most cases, a combination of electron diffraction and imaging was used to determine that the lamellar phase had been replaced by anatase. In rare cases, the product of reaction of anatase and the lamellae was rutile.

The transformation of X to anatase proceeded either by growth of subnanometer ledges of anatase along the interface between the two phases or by propagation of anatase at the expense of the second mineral along a broad front. Where narrow lamellae of the second phase (X) were contained within anatase, or where there was abundant anatase intergrown with the wide lamellae, the reaction tended to proceed by motion of steps. In some instances, the transformation occurred rapidly, and the interface appeared to jump suddenly through the sample, as shown by the comparison of Figure 4a with 4b. In regions predominantly composed of the second mineral, the bulk mechanism predominated.

Figure 5 shows the region visible in Figure 4, now oriented with the electron beam approximately parallel to [010] of anatase after the sample was transferred to a room temperature double-tilt holder. The area labeled A′ corresponds to an unreacted region in Figure 4a. A narrow strip of the unreacted phase (marked by an arrow and an X) has been preserved.

A partially reacted region present in the right part of Figure 5 is enlarged in Figure 6. This micrograph shows a thin lamella of anatase that has replaced the second phase (X) along a broad, but slightly serrated, front. On the right-hand side of this lamella, at least three ledges less than 1 nm high (marked by arrows) can be observed. Motion of these ledges along the boundary was observed at high temperature.

High-resolution electron microscopy

Through-focus series of images were obtained from the intergrowths in two orientations. Images recorded above and below the optimum defocus (−48 nm for the JEM 4000EX) for the [010] projection of anatase are shown in Figure 7, and the optimum defocus image from the [53$\bar{1}$] zone of anatase is shown in Figure 8. An image of the boundary between anatase and X is shown at greater magnification in Figure 9. Prolonged examination in the 400-keV microscope caused the growth of a different phase along the thin edge of the sample. This beam damage is illustrated in Figure 10.

Image simulation and distance-least-squares modeling

Anatase images were calculated for a range of crystal thickness and objective lens defocus values for the [010] and [53$\bar{1}$] zones. By matching the characteristics of the experimental images with these simulations, it was possible to establish the thickness and defocus conditions that were appropriate for the images of the intergrowths.

The optimum defocus images of anatase (Figs. 7c, 9) show that columns of pairs of Ti cations in the structure are clearly resolved. For this reason, we attributed pairs of similar spots in the image from the lamellae as representing columns of Ti cations. We measured the position of these columns within the unit cell suggested by electron diffraction and derived a model for the cation positions in the structure. Because of its low atomic scattering factor compared with that of Ti, O will contribute little contrast to the high-resolution images. Consequently, the projected positions of O atoms can not be determined directly from the images. However, calculation of images corresponding to a structure that contained only Ti cations indicated that the O atoms must contribute in a subtle way to the characteristics of high-resolution images in

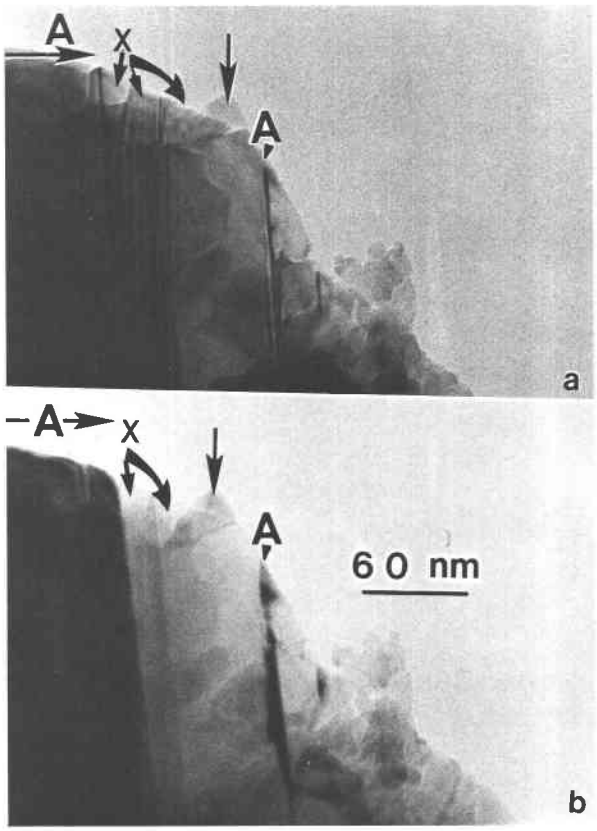

Fig. 4. Images of the intergrowths recorded approximately at 700 °C (furnace temperature) (**a**) immediately before, and (**b**) immediately after, the growth of the area of anatase (horizontal arrow) at the expense of the other polymorph (X). The vertical arrow marks a point of reference.

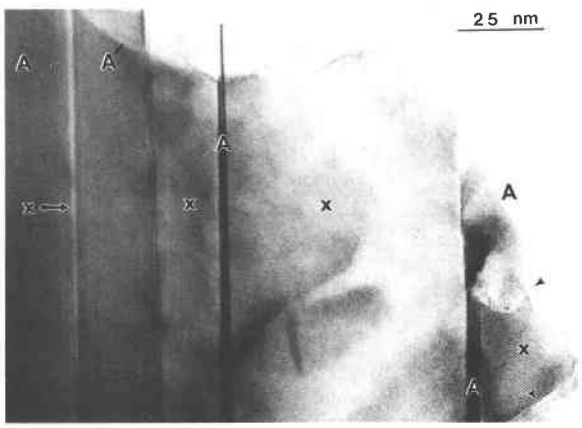

Fig. 5. Image of the area in Figure 4, after the sample was cooled, transferred to a double-tilt holder, and oriented in the [010] anatase projection. On the left side of the figure the arrowed strip of the second polymorph, marked with an arrow and X, was preserved after the area to the right was converted to anatase (A′). The small arrowheads (on the far right-hand side of the image) mark points shown in the enlargement of this area in Figure 6.

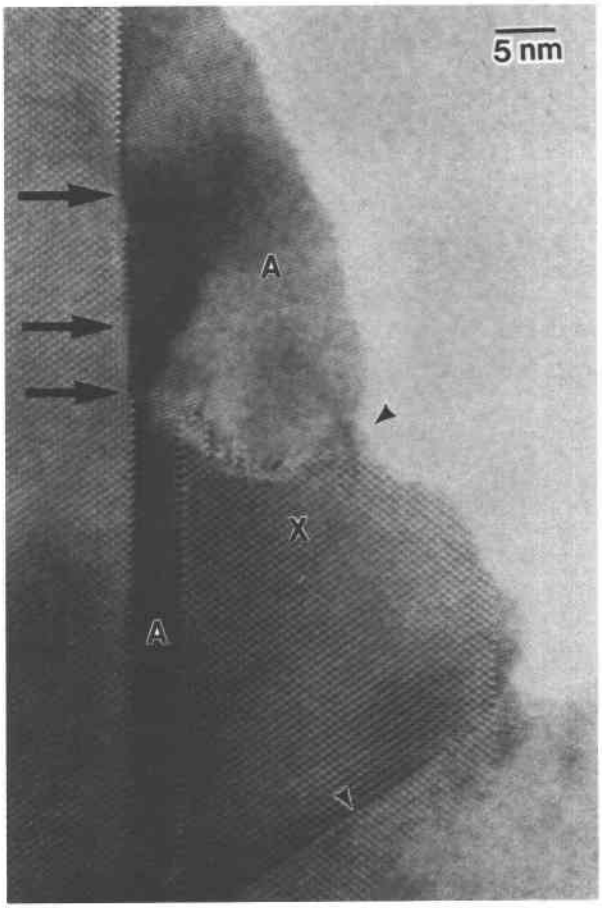

Fig. 6. Enlargement of the area marked in Figure 5 showing a strip of anatase that has replaced the other polymorph (X) along a wide front. Steps of anatase approximately 0.5 nm high (arrowed) were observed to grow along the interface at high temperature.

the [010] projection. This result suggests that matching fine details in the simulations for the model with details of the experimental images could provide reasonably reliable projected positions for the O atoms in the structure.

By analogy with anatase, rutile, and brookite, the structure of the unnamed mineral can be anticipated to be composed of octahedrally coordinated cations, with octahedra linked only by edge and corner sharing. This constraint led almost immediately to a single structure model, from which image simulations were generated for comparison with the experimental images in the through-focus series.

The moderately good match between the image simulations for the initial model and the experimental image at the optimum defocus is illustrated in Figure 11a. The most obvious discrepancy of detail is within the linear arrangement of small white spots. In the experimental image, the break between groups of three small white spots lies between two black spots (and offset from the largest white splotches), whereas, in the simulation, these breaks overlie the largest white splotches. Furthermore,

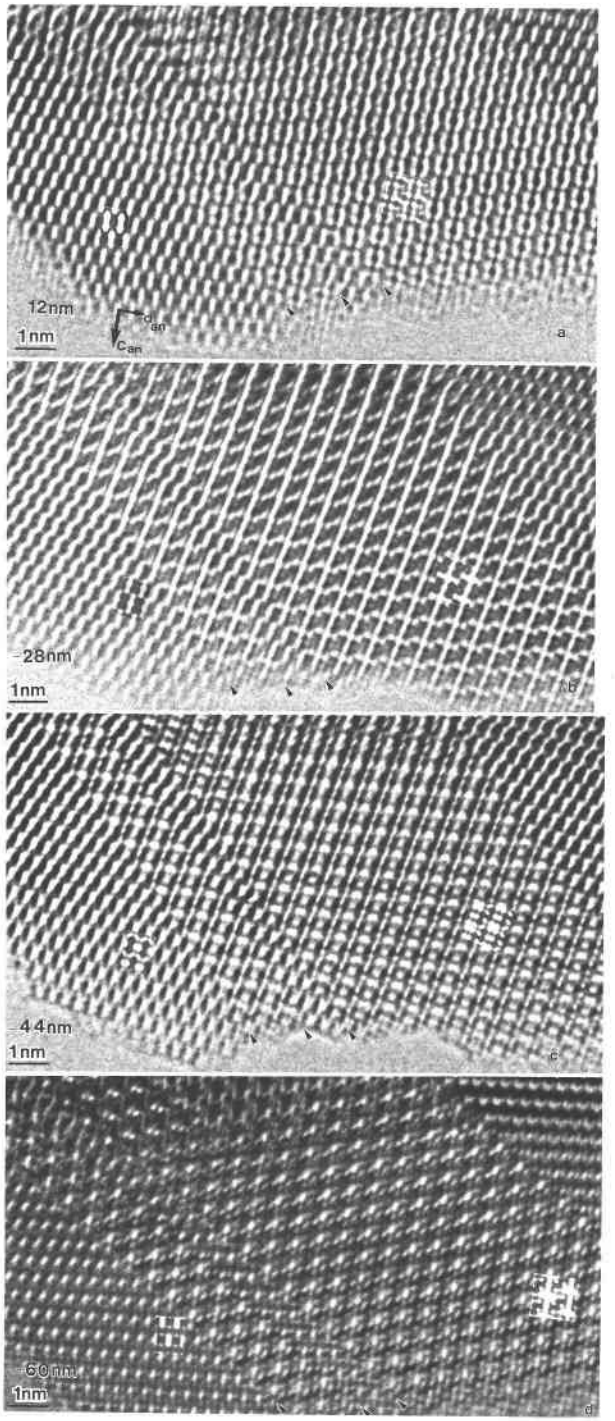

Fig. 7. Through focus series of [010] anatase with superimposed image simulations for anatase and the DLS-improved model structure (**a**) defocus 12 nm, thickness 2.5 nm; (**b**) defocus −28 nm, thickness 2.5 nm; (**c**) defocus −44 nm, thickness 2.5 nm; (**d**) defocus −60 nm, thickness 2.5 nm. Arrows show a defect in the new mineral (X) that can be seen in **c** to consist of a thin strip of anatase (A).

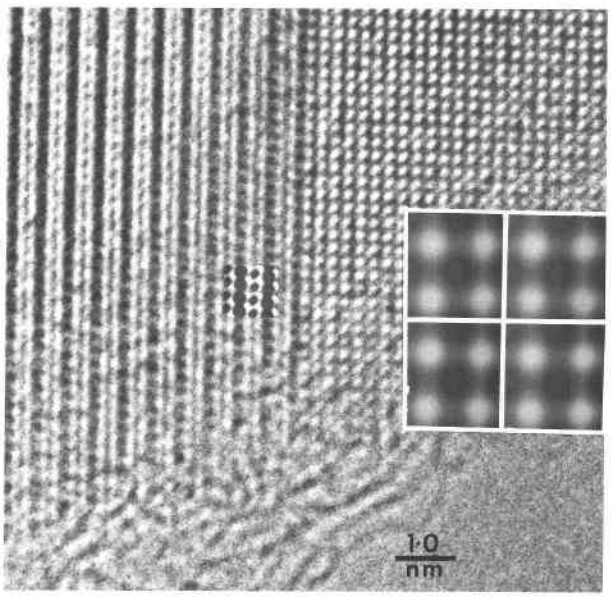

Fig. 8. Image in anatase [53$\bar{1}$] showing a lamella of the second polymorph and image simulations calculated for a defocus of −48 nm and crystal thickness of approximately 2.5 nm. The simulation for anatase is shown enlarged in the inset.

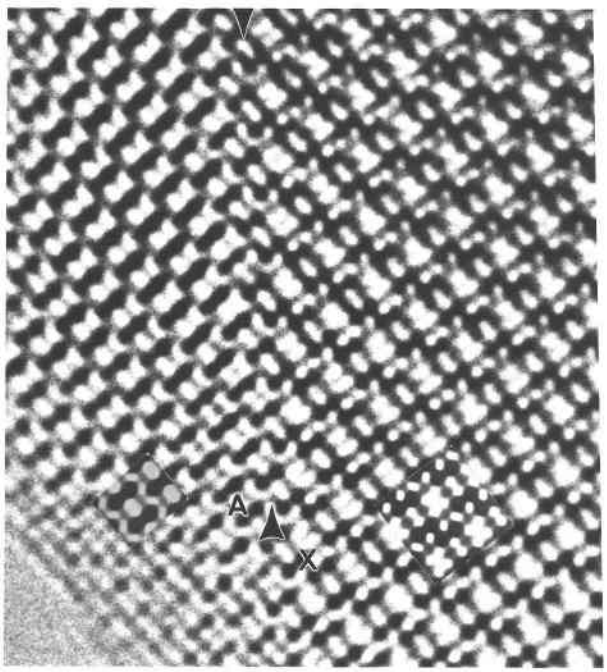

Fig. 9. Image of a lamella boundary and simulations for the structures of the two minerals. Careful examination [sighting at a low angle parallel to (001) anatase] of the arrangement of black spots (corresponding to columns of Ti cations) indicates that coherency is attained locally by small atomic displacements at the boundary.

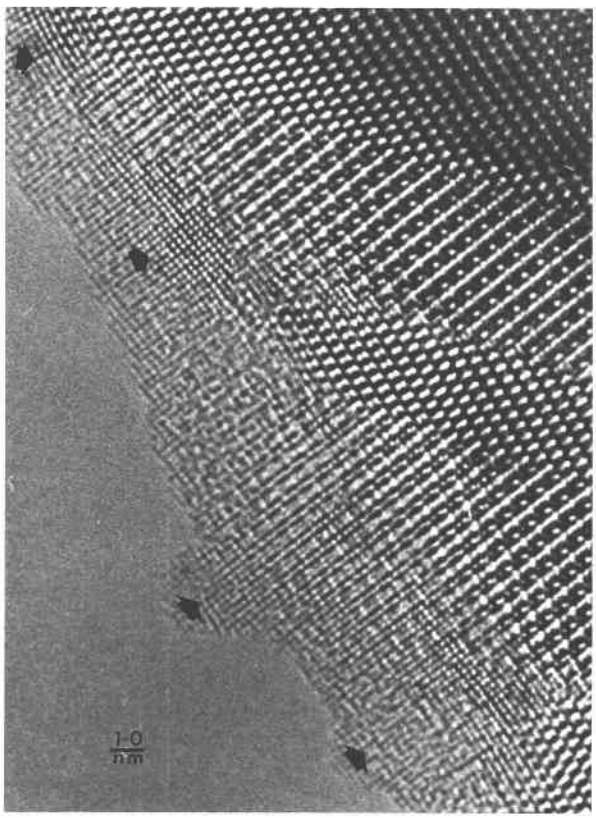

Fig. 10. Micrograph showing a crystalline product (arrowed) of TiO that resulted from electron-beam irradiation. The product has a square lattice and replaces both anatase and X, particularly at their interface.

the calculated interatomic distances for the initial model structure were rather variable, many of them being larger or smaller than those found in anatase, rutile, and brookite.

In order to adjust the atomic coordinates and thus improve the consistency between expected and model interatomic distances, we used a distance-least-squares calculation. This comparatively simple structure modeling approach has been used successfully in conjunction with X-ray diffraction to solve otherwise intractable problems (see review by Burnham, 1985). DLS should be an effective technique for optimizing TiO_2 structures, given the general topology and the size and shape of the unit cell, because of the number of existing polymorphs that all display relatively uniform Ti-Ti and Ti-O distances (however, the O-O distances for both shared and unshared edges are less predictable).

We tested this hypothesis by specifying a set of atomic coordinates (not related by symmetry) for anatase that were somewhat displaced from their known positions (up to 10%), allowing the program to adjust the interatomic distances to approach those found in rutile. Generally we found that the program converged on a set of coordinates within 1% of those found in the known structure. The

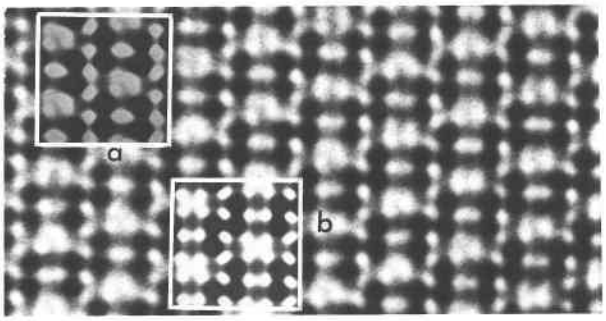

Fig. 11. Optimum-focus image and simulations (**a**) for the initial model of the unknown structure; (**b**) for the DLS-improved model structure.

convergence was not strongly dependent on the weights assigned to the distance specifications.

When applied to the model of the new structure, the program again rapidly converged regardless of whether the lengths for the shared edges were specified to be close to those in rutile or anatase. Modeling of the O-O distances by comparison with those found in the well-established polymorphs is complicated by the fact that they contain octahedra that share different numbers of edges, in a variety of configurations. We attempted to approach the most physically reasonable structure by adjusting the O-O distances to reflect these considerations (modeled with O-O unshared = 0.3 nm compared to 0.295 in rutile and 0.303 in anatase; O-O = 0.26 or 0.27 nm for shared edges, depending on the arrangement of shared edges, compared with O-O shared edges of 0.241, 0.254, 0.277 nm in anatase and rutile).

The phase grating calculated by the SHRLI image simulation package (see Fig. 12) shows the projected arrangement for the Ti (large black spots) and O atoms (small gray spots) for the final DLS-improved model (Fig. 11b).

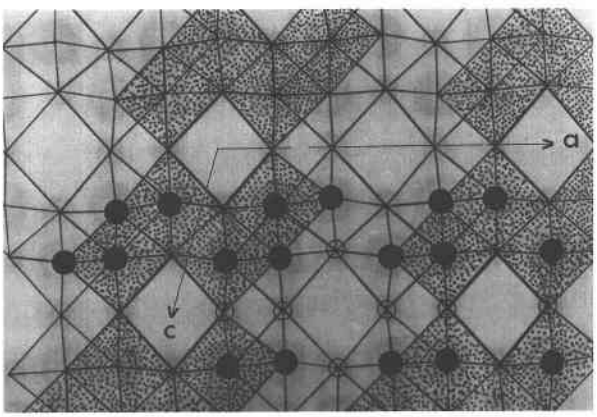

Fig. 12. Phase grating output from the SHRLI programs showing the projected positions of columns of Ti (large gray spots) and O atoms (smaller gray spots). Filled circles emphasizing the positions of the Ti atoms, open circles emphasizing the positions of the O atoms. Coordination polyhedra and axes are superimposed.

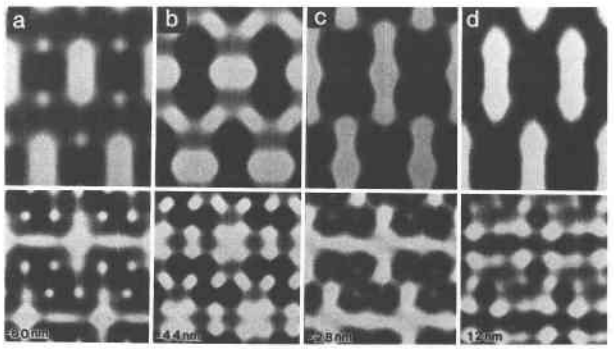

Fig. 13. Image simulations calculated for both anatase (upper set) and the DLS-improved model structure (lower set) at thicknesses of approximately 2.5 nm at defocuses of 12, −28, −44, and −60 nm.

The superimposed polyhedral diagram shows that this structure is composed of corner-linked pairs of edge sharing octahedra. These octahedra have a regular size and shape, and they have similar interatomic distances and volumes to those found in anatase and rutile.

The simulations calculated for [010] anatase at several defocus values and a thickness (2.5 nm) that matches the image characteristics at the edge of the sample (Fig. 7) are reproduced in Figure 13, together with the simulations for the model structure (at the same defocus values and thickness). In Figures 7 and 8, these simulations have been superimposed onto the experimental images. The matches for all examples are quite good. The detailed match of the [010] optimum defocus image (Fig. 11b) is much improved relative to that for the initial model (Fig. 11a); the break between groups of three white spots is now positioned correctly. Furthermore, the simulations show areas with lighter contrast corresponding to O atom positions (see phase grating in Fig. 12) that duplicate regions with light contrast in the high-resolution images.

Table 3 illustrates the comparison between the idealized structure (no polyhedral distortion; as reported by Catlow et al., 1984), the TiO_2 (B) structure predicted by energy minimization modeling (Catlow et al., 1984), and the DLS-optimized TEM structure for the mineral referred to above as X. Because the DLS-structure was modeled using a primitive rather than C-centered unit cell, duplicate results for equivalent positions were obtained.

For the VO_2 structure, Catlow et al. (1984) report δ values for the atomic coordinates (powder X-ray minus ideal) of 0.01–0.07 and between the energy minimization and X-ray structures of less than 0.01–0.04. For the TiO_2 (B) structure, the differences between the (x, z) coordinates of the ideal and DLS-optimized structure (average values) range between 0.0 and 0.03, and those between the energy minimization and DLS structure range between 0.00 and 0.06 (all except one result that is within 0.04). In every case in which the DLS-optimized coordinates are not intermediate between those of the ideal and energy-minimized structures, they are equal to them.

Table 3. The (x, z) coordinates for the 4i site ($C2/m$) for the idealized VO_2 structure, the lattice-energy-minimization-predicted structure (LEM), and the DLS-modeled primitive structures

Site		Idealized*	LEM*	DLS**
Ti(1)	x	0.22	0.18	(a) 0.22
	z	0.33	0.28	0.33
				(b) 0.20
				0.31
Ti(2)	x	0.38	0.40	(a) 0.40
	z	0.33	0.26	0.33
				(b) 0.38
				0.31
O(1)	x	0.67	0.63	(a) 0.66
	z	0.00	0.01	0.01
				(b) 0.66
				0.00
O(2)	x	0.22	0.24	(a) 0.25
	z	0.33	0.34	0.35
				(b) 0.23
				0.31
O(3)	x	0.45	0.44	(a) 0.45
	z	0.67	0.63	0.65
				(b) 0.43
				0.63
O(4)	x	0.61	0.65	(a) 0.63
	z	0.67	0.72	0.69
				(b) 0.62
				0.66

Note: (a) and (b) are independent results for equivalent sites in the C-centered unit cell.
* Catlow et al. (1984).
** Average for three DLS calculations.

Discussion

The structure of the unnamed mineral in the lamellae (X) in anatase was determined by electron microscopic and modeling techniques. This study has established that X is the equivalent of the synthetic Ti-oxide known as TiO_2 (B), and thus that TiO_2 (B) occurs in nature.

The TiO_2 (B) mineral converted to anatase on heating, suggesting either that it primarily contained tetravalent Ti or that interaction of the electron beam caused oxidation of trivalent Ti in the structure. Both the results of previous studies on TiO_2 beam damage and the results of this study (discussed below) suggest that damage involves reduction rather than oxidation of the specimen. Consequently, the heating experiments are interpreted to indicate that TiO_2 (B) primarily contains tetravalent Ti. It would be unusual indeed to find appreciable trivalent Ti in metamorphic rocks such as those from which the samples were taken.

The possibility that the lamellae could have formed as a result of electron irradiation during examination was tested by deliberately exposing the intergrowths to a high and prolonged electron dose (in the 400-keV JEM 4000EX). No evidence was found to suggest that the beam promoted the development of TiO_2 (B). Indeed, an alternative crystalline product developed from both TiO_2 (B) and anatase along the edge of the sample (Fig. 10). This reaction product has spacings of approximately 0.21 nm between its square lattice fringes, consistent with its identification as TiO (NaCl structure). This product devel-

oped on both the anatase and TiO_2 (B), reflecting the tendency of the electron beam to reduce the Ti in both minerals.

The development of TiO as a result of beam damage (radiolysis) of TiO_2 (rutile) has been previously described by Smith et al. (1987). McCartney and Smith (1989) also noted the development of TiO_2 II, the high-pressure phase, as a result of electron irradiation of rutile. This interesting and rather surprising observation was not made in the damaged anatase and TiO_2 (B). Figure 10 shows that the TiO develops preferentially at the interface between TiO_2 (B) and anatase. This probably indicates that the interface has a higher reactivity because of the coherency strain associated with it.

The identification of TiO_2 (B) as intimate intergrowths in anatase suggests that these minerals are genetically related in nature. Although we have no evidence as to how common the TiO_2 (B) polymorph is, Banfield (1990) demonstrated that it does develop in the weathering environment. TiO_2 (B) may form commonly in nature at low temperatures. The study of sample B6134 by J. Post (personal communication) indicates that although TiO_2 (B) may comprise a very small proportion of a sample, this mineral is sufficiently abundant that it can be identified by powder X-ray diffraction.

By comparing the image simulations with the experimental image in Figure 9, the structure of the boundary between TiO_2 (B) and anatase can be inferred. Electron diffraction patterns indicate that there is some misfit between the two lattices parallel to their interface. This was also noted by Brohan et al. (1982), who observed that partly reacted synthetic crystals of TiO_2 (B) are subdivided into small domains that are believed to have formed as a result of this misfit. Examination of grain boundaries in the samples described here indicates that despite the differences between the lattice parameters, the interfaces contain broad areas of coherency. Figure 9 illustrates distortion or slight atomic displacements that occur at the boundary. Although the simplified diagram of the boundary (Fig. 14) does not show this distortion, it does illustrate that the boundary region is highly structured, with many polyhedra shared by both phases. The arrangement of dark spots in Figure 14 can be compared with those in the high-resolution image (Fig. 9). The dashed line marking the boundary between TiO_2 (B) and anatase in Figure 14 marks the furthest extent of polyhedra in an arrangement consistent with the anatase structure. The boundary could be considered to (approximately) extend across the region shown to contain polyhedra common to both structures.

The TiO_2 (B) polymorph is known to have a structure that is systematically related to that of anatase (Brohan et al., 1982). It has been shown that the synthetic material converts to anatase with increasing temperature (Brohan et al., 1982). Brohan et al. reported that samples transformed as a result of either increased temperature or pressure (550 °C and 1 atm, or 60 kbar and room temperature). Our heating experiments demonstrated that the

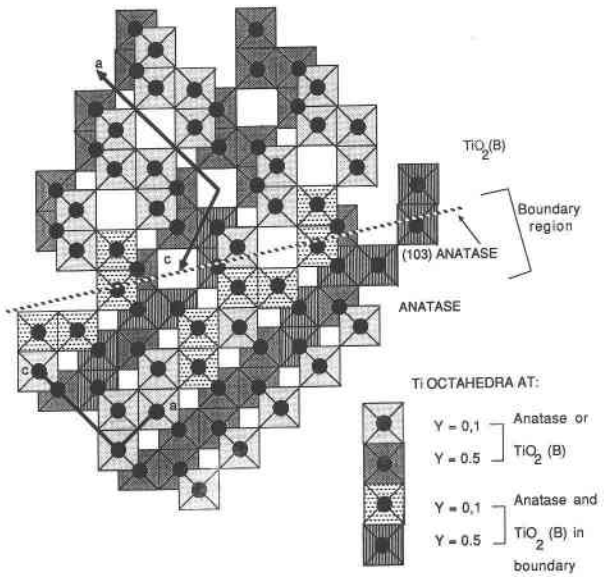

Fig. 14. Polyhedral representation of the structure of anatase, TiO_2 (B), and their boundary. Black dots mark positions of Ti atoms; compare the arrangement at the boundary with that seen in Figure 9.

reaction can be induced in situ in the microscope under low-pressure conditions. In nature, the reaction almost certainly proceeds at much lower temperatures, probably only partly as a result of the greater pressure (a few kilobars).

Brohan et al. (1982) proposed a TiO_2 (B) → anatase transformation mechanism based on the identified topotactic relationship and the observation that anatase can be derived from the TiO_2 (B) phase by a process similar to crystallographic shear in the Magnéli phases, with the shear eliminating equal numbers of cationic and anionic vacancies.

Our in situ observations of the TiO_2 (B) → anatase reaction indicate that it may proceed either by growth of individual steps on the lamellar margins or by movement of a front through the sample, which occurs at times quite rapidly. The transformation by growth of steps is generally in accord with the mechanism proposed by Brohan et al. (1982), insofar as the transformation involves systematic displacement of octahedra parallel to the boundary. Dynamic observations, as well as micrographs from the quenched reaction (Fig. 6), suggest that this process occurs by growth of steps approximately 0.5 nm high. Our interpretation of the mechanism, illustrated in Figure 15, indicates that these steps correspond to the slabs that must be displaced to create one structure from the other.

The TiO_2 (B) lamellae may either have formed by simultaneous growth with anatase or have remained after the incomplete prograde replacement of TiO_2 (B) by anatase. It is probable that with increasing temperature, anatase in nature would completely replace TiO_2 (B), as it did in our experiments. Two sequential reactions antici-

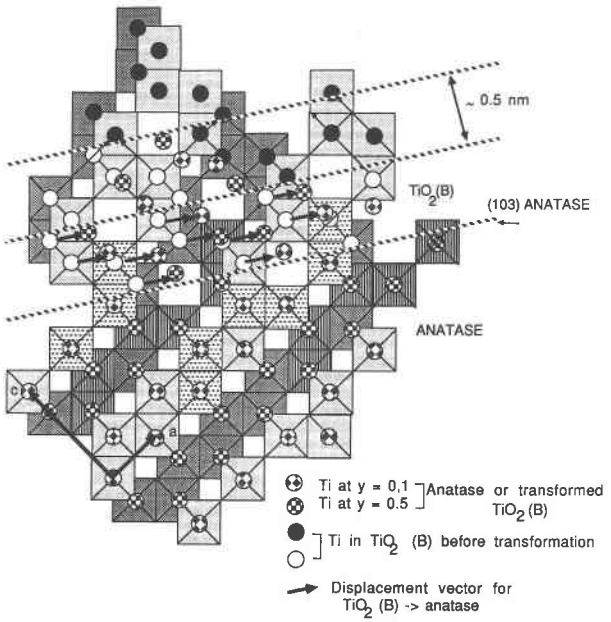

Fig. 15. Diagram illustrating the displacement that relates the two structures. The width of the displaced slabs corresponds to the height of the anatase ledges during the transformation.

pated in low-grade metamorphic rocks are the transformation of TiO_2 (B) → anatase and anatase → rutile.

Laboratory transformation of anatase to rutile occurs at high temperature. Rao (1961) stated that below approximately 610 °C the transformation is infinitely slow. We can infer from the observations of Hunziker et al. (1986) and others that the anatase → rutile transformation probably occurs at temperatures below approximately 400 °C in metapelites from the Swiss Alps. Although the exact temperatures of the TiO_2 (B) → anatase and anatase → rutile transformations will largely reflect kinetic factors (Shannon and Pask, 1965, showed that the anatase → rutile transformation temperature is strongly influenced by impurities and defect), we anticipate that they will occur sequentially in low-grade metamorphic rocks.

It has been often suggested that rutile, anatase, and brookite form as weathering products of Ti-bearing minerals such as biotite (Morad and Aldahan, 1982), amphibole, pyroxene (Loughnan, 1969), and ilmenite (Grey and Reid, 1975). Other possible precursors include amorphous Ti-oxide or $Ti(OH)_4$ (Loughnan, 1969). It is interesting to note that TiO_2 (B) can be synthesized by dehydration and structural rearrangement of $H_2Ti_4O_9 \cdot H_2O$ (Tournoux et al., 1986). Feist et al. (1988) further discuss synthesis from a variety of structurally related Na and Cs compounds via intermediate H compounds. We suggest that, if analogous hydrous Ti-oxide compounds occur in nature, their dehydration and collapse during diagenesis or very low-grade metamorphism may result in the formation of TiO_2 (B) and, by extension, anatase and rutile in metamorphic rocks.

Conclusions

This study has shown that the structure of a mineral that occurs in submicroscopic quantities can be determined using an approach that combines AEM, electron diffraction, high-resolution imaging, image simulations, and DLS refinement. Image simulation showed that the positions of columns of Ti cations could be readily determined from the high-resolution images and that the distribution of diffuse intensity in optimum-defocus images could provide a first estimate for the anion positions. DLS refinement of the initial model resulted in a structure containing polyhedra similar to those found in anatase and rutile. A very close match between the simulated images for the DLS-optimized structure and experimental images was demonstrated. Not only did the DLS-optimized structure correspond to the general structure of the synthetic phase TiO_2 (B), but the octahedral distortions from the ideal structure closely resembled those predicted for TiO_2 (B) using energy minimization techniques (Catlow et al., 1984).

The unnamed mineral represents the fourth naturally occurring TiO_2 polymorph. It is known that TiO_2 (B) can be synthesized by dehydration and collapse of a hydrous precursor. Consequently, it is possible that reactions converting similar precursor compounds to TiO_2 (B) in nature represent the first steps that may result in the formation of up to three TiO_2 polymorphs in low-grade rocks (all polymorphs may also be formed directly in some cases). Further systematic study is needed to establish how common the TiO_2 (B) polymorph is. Given the probable irreversible nature of the reactions TiO_2 (B) → anatase and anatase → rutile, these minerals may prove useful indicators of peak metamorphic temperatures in low-grade rocks.

Acknowledgments

Thanks are expressed to Ken Livi for providing the initial anatase sample, discussions, and microprobe data; to Renu Sharma for discussion of the chemical literature; to Jeff Post for assistance with the DLS program, access to powder X-ray diffraction results, and discussion; to M. O'Keefe for providing the SHRLI software; and to Stefan Graeser for information on the geological history of the anatase-bearing rocks. Dimitri Sverjenski, George Guthrie, and Peter Davies provided constructive comments on the manuscript. Tamsin McCormick is thanked for her review and editorial help. This research was supported by NSF grants EAR-8609277, EAR-8903630, and DMR-8611609.

References cited

Banfield, J.F. (1990) HRTEM studies of subsolidus alteration, weathering, and subsequent diagenetic and low-grade metamorphic reactions. Ph.D. thesis, Johns Hopkins University, Baltimore, Maryland.

Baur, W.H. (1961) Atomabstände und bindungswinkel im brookit, TiO_2. Acta Crystallographica, 14, 214–216.

Brohan, L., Verbaere, A., Tournoux, M., and Demazeau, G. (1982) La transformation TiO_2 (B) → anatase. Material Research Bulletin, 17, 355–361.

Burnham, C. W. (1985) Mineral structure energetics and modeling using the ionic approach. Microscopic to macroscopic. In Mineralogical Society of America Reviews in Mineralogy, 14, 347–388.

Catlow, C.R.A., Cormack, A.N., and Theobald, F. (1984) Structure pre-

diction of transition-metal oxides using energy minimization techniques. Acta Crystallographica, B40, 195–200.

Cromer, D.T., and Herrington, K. (1955) The structures of anatase and rutile. Journal of the American Chemical Society, 77, 4708–4709.

Feist, T.P., Mocarski, S.J., Davies, P.K., Jacobson, A.J., and Lewandowski, J.T. (1988) Formation of TiO_2 (B) by proton exchange and thermolysis of several alkali metal titanate structures. Solid State Ionics, 28–30, 1338–1343.

Grey, I., and Reid, F. (1975) The structure of pseudorutile and its role in the natural alteration of ilmenite. American Mineralogist, 60, 898–906.

Hunziker, J.C., Frey, M., Clauer, N., Dallmeyer, R.D., Friedrichsen, H., Flehmig, W., Hochstrasser, K., Roggwiler, P., and Schwanderm H. (1986) The evolution of illite to muscovite; mineralogical and isotopic data from Glarus Alps, Switzerland. Contributions to Mineralogy and Petrology, 92, 157–180.

Latroche, M., Brohan, L., Marchand, R., and Tournoux, M. (1989) New hollandite oxides; TiO_2 (H) and $K_{0.06}TiO_2$. Journal of Solid State Chemistry, 81, 78–82.

Loughnan, F. (1969) Chemical weathering of silicate minerals, 154 p. Elsevier, New York.

Marchand, R., Brohan, L., and Tournoux, M. (1980) TiO_2 (B), a new form of titanium dioxide and the potassium octatitanate $K_2Ti_8O_{17}$. Material Research Bulletin, 15, 1129–1133.

McCartney, M.R., and Smith, D.J. (1989) Epitaxial relationships in electron-stimulated desorption processes at transition metal oxide surfaces. Surface Science, 221, 214–232.

Morad, S., and Aldahan, A.A. (1982) Authigenesis of titanium minerals in two Proterozoic sedimentary rocks from southern and central Sweden. Journal of Sedimentary Petrology, 52, 1295–1305.

O'Keefe, M.A. (1984) Electron image simulation: A complementary processing technique. In J.J. Hren, F.A. Lenz, E. Munro, and P.B. Sewell, Eds., Electron optical systems, p. 209–220. SEM Inc., AMF O'Hare, Chicago, Illinois.

O'Keefe, M.A., Buseck, P.R., and Iijima, S. (1978) Computed crystal structure images for high resolution electron microscopy. Nature, 274, 322–324.

Rao, C.N.R. (1961) Kinetics and thermodynamics of the crystal structure transformation of spectroscopically pure anatase to rutile. Canadian Journal of Chemistry, 39, 498–500.

Self, P.G., and O'Keefe, M.A. (1988) Calculation of diffraction patterns and images for fast electrons. In P.R. Buseck, J.M. Cowley, and L. Eyring, Eds., High-resolution transmission electron microscopy, p. 244–307. Oxford University Press, Oxford, United Kingdom.

Shannon, R.D., and Pask, J.A. (1965) Kinetics of the anatase-rutile transformation. Journal of the American Ceramics Society, 48, 391–398.

Simons, P.Y., and Dachille, F. (1967) The structure of TiO_2-II, a high pressure phase of TiO_2. Acta Crystallographica, 23, 334–335.

Smith, D.J., McCartney, M.R., and Bursill, L.A. (1987) The electron-beam-induced reduction of transition metal oxide surfaces to metallic lower oxides. Ultramicroscopy, 23, 299–304.

Theobald, F.R., Catlow, C.R.A., and Cormack, A.N. (1984) Lattice energy minimization as a complementary technique to refine structures obtained by high-resolution electron microscopy. Journal of Solid State Chemistry, 52, 80–90.

Tournoux, M., Marchand, R., and Brohan, L. (1986) Layered $K_2Ti_4O_9$ and the open metastable TiO_2 (B) structure. Progress in Solid State Chemistry, 17, 33–52.

Manuscript received June 20, 1990
Manuscript accepted January 7, 1991